Air-sea exchange in the global mercury cycle

Sarah A. Strode,[1] Lyatt Jaeglé,[1] Noelle E. Selin,[2] Daniel J. Jacob,[2] Rokjin J. Park,[2] Robert M. Yantosca,[2] Robert P. Mason,[3] and Franz Slemr[4]

Received 21 May 2006; revised 20 September 2006; accepted 17 October 2006; published 17 March 2007.

[1] We present results from a new global atmospheric mercury model coupled with a mixed layer slab ocean. The ocean model describes the interactions of the mixed layer with the atmosphere and deep ocean, as well as conversion between elemental, divalent, and nonreactive mercury species. Our global mean aqueous concentrations of 0.07 pM elemental, 0.80 pM reactive, and 1.51 pM total mercury agree with observations. The ocean provides a 14.1 Mmol yr^{-1} source of mercury to the atmosphere, at the upper end of previous estimates. Re-emission of previously deposited mercury constitutes 89% of this flux. Ocean emissions are largest in the tropics and downwind of industrial regions. Midlatitude ocean emissions display a large seasonal cycle induced by biological productivity. Oceans contribute 54% (36%) of surface atmospheric mercury in the Southern (Northern) Hemisphere. We find a large net loss of mercury to the deep ocean (8.7 Mmol yr^{-1}), implying a ~0.7%/year increase in deep ocean concentrations.

Citation: Strode, S. A., L. Jaeglé, N. E. Selin, D. J. Jacob, R. J. Park, R. M. Yantosca, R. P. Mason, and F. Slemr (2007), Air-sea exchange in the global mercury cycle, *Global Biogeochem. Cycles*, *21*, GB1017, doi:10.1029/2006GB002766.

1. Introduction

[2] Atmospheric mercury deposited to aquatic surfaces can convert to methyl mercury, a highly toxic species that bioaccumulates in the aquatic food chain. This results in human exposure to hazardous levels of mercury in seafood [*National Research Council*, 2000], as well as detrimental effects on wildlife [*Wolfe et al.*, 1998]. Because mercury is transported over long distances in the atmosphere, these effects occur even in ecosystems remote from local sources [*Lindqvist et al.*, 1991].

[3] Mercury is emitted to the atmosphere from anthropogenic sources, such as fossil fuel combustion, metal and cement production, waste incineration, and chemical plants [*Pacyna et al.*, 2003], with direct anthropogenic emissions representing approximately one third of the total [*Mason and Sheu*, 2002]. The remaining emissions come from land and ocean sources, each accounting for about a third of global mercury emissions. Mercury is removed from the atmosphere via wet and dry deposition, with an overall lifetime of 0.5–2 years [*Schroeder and Munthe*, 1998]. The effect of anthropogenic emissions is evident in the sediment record, which shows a factor of 2–3 increase in mercury deposition since the onset of the industrial era [*Fitzgerald et al.*, 1998, and references therein], as well as in measurements showing atmospheric concentration increasing by 1.2–1.5% yr^{-1} from 1977–1990 [*Slemr and Langer*, 1992]. *Mason and Sheu* [2002] estimate that since the pre-industrial age the atmospheric burden and deposition of mercury have increased by a factor of 3, while land and ocean emissions have doubled owing to reemission of anthropogenic mercury. Since 1990, a decreasing trend in atmospheric mercury concentrations has been observed [*Slemr et al.*, 1995, 2003].

[4] Exchange between the atmosphere and ocean plays an important role in the cycling and transport of mercury. Atmospheric deposition is the main source of mercury to the ocean, and therefore affects the oceanic distribution of aqueous mercury. Conversely, the ocean reemits mercury to the atmosphere as a result of supersaturation of dissolved gaseous mercury in the ocean with respect to the air [*Schroeder and Munthe*, 1998]. Oceanic emissions may thus contribute to the long-range transport of atmospheric mercury through a "multihop" mechanism as atmospheric mercury is deposited to the ocean and then reemitted to the atmosphere [*Schroeder and Munthe*, 1998; *Hedgecock and Pirrone*, 2004].

[5] There are a number of uncertainties in the ocean source, including not only its total magnitude but also its spatial and seasonal distribution. The global sea-air flux of mercury is estimated to lie between 4 and 13 Mmol yr^{-1} (Table 1) [*Fitzgerald*, 1986; *Kim and Fitzgerald*, 1986;

[1]Department of Atmospheric Sciences, University of Washington, Seattle, Washington, USA.
[2]Division of Engineering and Applied Sciences and Department of Earth and Planetary Sciences, Harvard University, Cambridge, Massachusetts, USA.
[3]Department of Marine Sciences, University of Connecticut, Groton, Connecticut, USA.
[4]Air Chemistry Division, Max-Planck-Institute for Chemistry, Mainz, Germany.

0886-6236/07/2006GB002766$12.00

Table 1. Global Budgets of Mercury in the Mixed Layer

	Mason et al. [1994a]	*Mason and Sheu* [2002]	*Lamborg et al.* [2002]	This Study
Sources, Mmol yr^{-1}				
Atmospheric deposition	10	15.4	10	22.8
Riverine input	1	1	0	0
Sinks, Mmol yr^{-1}				
Net Flux to atmosphere	10	13	4	14.1
Net loss to deep ocean	1	3.4	6	8.7
Mixed layer burden, Mmol	54	360	54	34
Mixed layer depth, m	100	500	100	53[a]

[a]Average mixed layer depth.

Lindqvist et al., 1991; *Mason et al.*, 1994a; *Hudson et al.*, 1995; *Lamborg et al.*, 2002; *Mason and Sheu*, 2002]. Open-ocean fluxes calculated from measurements during individual cruises range from 600 ng m^{-2} $month^{-1}$ in the North Pacific in May [*Laurier et al.*, 2003] to 60,000 ng m^{-2} $month^{-1}$ in the Equatorial and South Atlantic in May and June [*Lamborg et al.*, 1999]. This large regional and temporal variability appears to be a function of local wind speed, temperature, aqueous mercury concentration, and biological activity. It has been suggested that the cycling of mercury between ocean and atmosphere could be further influenced by the rapid formation of reactive gaseous mercury in the marine boundary layer in the presence of sea salt aerosol [e.g., *Hedgecock and Pirrone*, 2001].

[6] Several recent global models have advanced our understanding of the global atmospheric mercury distribution. Global models have provided insight into the relative importance of gas-phase oxidants such as ozone and OH [*Bergan and Rodhe*, 2001], as well as the effects of cloud chemistry [*Shia et al.*, 1999] and meteorological variability [*Dastoor and Larocque*, 2004]. These models have helped constrain the lifetime of mercury and the magnitude of emissions and deposition [*Bergan et al.*, 1999; *Shia et al.*, 1999], estimate the increase in deposition since the pre-industrial era [*Bergan et al.*, 1999], and attribute deposition to local and distant sources [*Seigneur et al.*, 2004]. Comparison of model and observations of reactive gaseous mercury (RGM) and total gaseous mercury (TGM) demonstrates the importance of photoreduction of RGM and a possible sea-salt sink in the marine boundary layer, and suggests a long lifetime for RGM at high altitude [*Selin et al.*, 2007].

[7] Uncertainties in the magnitude and seasonality of the ocean source pose a challenge for understanding the budget and distribution of mercury. To explain discrepancies between model and observations, *Bergan et al.* [1999] suggest that either the ratio of manmade to natural emissions is too low, or that there are large variations in the natural mercury cycle. Current global models assume that the ocean source is constant in time and space [*Shia et al.*, 1999], varies smoothly as a function of latitude without seasonal variation [*Bergan and Rodhe*, 2001; *Seigneur et al.*, 2001], or do not include ocean emissions [*Dastoor and Larocque*, 2004].

[8] Here we describe a new global simulation of mercury that couples the GEOS-Chem global atmospheric chemistry model with a mixed layer slab ocean model. The atmospheric mercury model is described in a separate paper [*Selin et al.*, 2007]. This is the first time that a global chemical transport model incorporates a fully coupled simulation of air-sea exchange of mercury. Section 2 of this paper presents observations of aqueous mercury used to validate our simulation, and section 3 describes the slab ocean model. We present results in section 4, where we describe the budget of mercury in the ocean, compare our results to observations, constrain air-sea exchange of mercury and examine its impact on atmospheric concentrations.

2. Observations

[9] Aqueous mercury in ocean waters is present in the form of elemental mercury (Hg^0_{aq}), monomethyl mercury (CH_3Hg^+), dimethyl mercury ($(CH_3)_2Hg$), aqueous divalent mercury (Hg^{II}_{aq}), colloidal mercury, and particulate mercury [*Morel et al.*, 1998]. Aqueous mercury measurements are frequently reported as dissolved gaseous mercury (DGM), reactive mercury, or total mercury. DGM includes both Hg^0_{aq} and $(CH_3)_2Hg$. Reactive mercury is experimentally defined as the mercury that can be reduced and/or volatilized from solution after addition of $SnCl_2$. It is considered to be the sum of Hg^0_{aq} and Hg^{II}_{aq} [*Mason et al.*, 1998], and includes inorganic mercury ions and kinetically facile organic complexes [*Lamborg et al.*, 2003]. For total mercury concentrations, samples are stored in acid solution for an extended time period so that more mercury is released from organic compounds and included in the measurement [*Gill and Fitzgerald*, 1987], or the samples are oxidized with bromine monochloride so that all dissolved, particulate, and colloidal mercury is included.

[10] Globally, total mercury concentrations in the surface ocean are estimated to be approximately 1.5 picomolar (1 pM = 10^{-12} moles $liter^{-1}$) [*Lamborg et al.*, 2002]. However, *Gill and Fitzgerald* [1987] reported values as high as 9.6 pM, while measurements in Bermuda [*Mason et al.*, 2001] show values below 1 pM. Tables S1, S2, and S3 in the auxiliary material[1] show a compilation of elemental, reactive, and total mercury observations used in this study. Reactive mercury comprises a major fraction of total mercury in the surface waters of the open ocean, with

[1]Auxiliary materials are available at ftp://ftp.agu.org/apend/gb/2006gb002766.

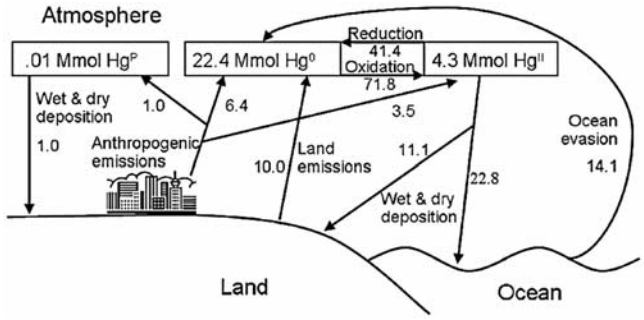

Figure 1. Global atmospheric budget for the standard GEOS-Chem simulation. All fluxes are in Mmol yr^{-1}.

average values ranging from 30 to 60% [*Coquery and Cossa*, 1995; *Mason and Sullivan*, 1999; *Horvat et al.*, 2003]. The fraction of reactive mercury as Hg^0_{aq} ranges from 45 to 100% in the Atlantic [*Mason et al.*, 1998; *Mason and Sullivan*, 1999], and 3 to 45% in the surface waters of the equatorial Pacific [*Mason and Fitzgerald*, 1993]. Colloidal mercury represents 10–50% of the open ocean concentrations [*Guentzel et al.*, 1996; *Mason and Sullivan*, 1999], and particulate mercury comprises 3–30% [*Coquery and Cossa*, 1995; *Mason and Sullivan*, 1999]. The concentration of methylated species is below the detection limit in the surface waters [*Cossa et al.*, 1994; *Mason and Fitzgerald*, 1993; *Mason and Sullivan*, 1999].

[11] Mercury enters the ocean mixed layer primarily through atmospheric deposition [*Gill and Fitzgerald*, 1987; *Mason et al.*, 1994a], with an additional contribution from upwelling and mixing from below [*Kim and Fitzgerald*, 1986; *Mason et al.*, 1994b]. Within the ocean mixed layer, mercury cycles between Hg^0_{aq}, Hg^{II}_{aq}, particulate, and organic forms [*Mason et al.*, 1994a; *Morel et al.*, 1998]. In productive regions, mercury can exit the mixed layer through conversion of reactive mercury to particulate form followed by particle settling [*Mason and Fitzgerald*, 1996]. Competing with this process is the reduction of Hg^{II}_{aq} to Hg^0_{aq}, which can be photochemically [*Amyot et al.*, 1997; *Costa and Liss*, 1999; *Rolfhus and Fitzgerald*, 2004] and/or biologically [*Mason et al.*, 1995; *Rolfhus and Fitzgerald*, 2004] mediated.

3. Model Description

3.1. General Description

[12] This study uses the GEOS-Chem global model of tropospheric chemistry [*Bey et al.*, 2001], which is driven by assimilated meteorological observations from the Goddard Earth Observing System (GEOS) of the NASA Global Modeling and Data Assimilation Office (GMAO). We conducted a mercury simulation for 2003 using GEOS-4 meteorological fields that have a horizontal resolution of $1° \times 1.25°$, 55 vertical levels and a temporal resolution of 6 hours (3 hours for mixing depths and surface quantities). We regrid these meteorological fields to $4° \times 5°$ and 30 vertical levels for computational expediency. GEOS-Chem is a fully forward Eulerian model. We run the model for 4 years, long enough to reach steady state, and use only the final year for analysis. We use GEOS-Chem version 7-04-01 (http://www.as.harvard.edu/chemistry/trop/geos/).

[13] The new atmospheric mercury simulation is described and evaluated by *Selin et al.* [2007]. Briefly, the model contains three tracers for atmospheric mercury: elemental (Hg^0), reactive (Hg^{II}), and particulate (Hg(P)) (Figure 1). Anthropogenic mercury emissions are taken from the Global Emissions Inventory Activity for 2000 (J. Pacyna et al., Spatially distributed inventories of global anthropogenic emissions of mercury to the atmosphere, 2005, available at www.amap.no/Resources/HgEmissions/), and account for 10.9 Mmol/yr. Land emissions are divided into a natural component of 2.5 Mmol/yr over naturally enriched soils, and a reemission component of 7.5 Mmol/yr distributed following atmospheric mercury deposition. Ocean emissions are calculated within the coupled model as 14.1 Mmol/yr. In the atmosphere, Hg^0 is oxidized in the gas phase by O_3 [*Hall*, 1995] and OH [*Sommar et al.*, 2001], and in cloudy regions, Hg^{II} undergoes aqueous-phase reduction to Hg^0. There is no interaction between modeled Hg^{II} and Hg(P), so these species are considered together when compared to measurements. Atmospheric mercury is lost via wet (11.4 Mmol/yr) and dry (23.4 Mmol/yr) deposition of Hg^{II} and Hg(P). Dry deposition is enhanced in the marine boundary layer by a first-order sink on sea salt aerosols. The resulting global atmospheric lifetimes are 4 months for Hg^0 against oxidation, 9.5 months for TGM (the sum of Hg^0 and Hg^{II}) against Hg^{II} deposition, and 3 days for Hg(P) against deposition.

[14] GEOS-Chem has no mean bias in TGM concentrations compared to land observations, and accounts for 51% of the variance in TGM measurements [*Selin et al.*, 2007]. Over the United States, the modeled wet deposition reproduces observations from the Mercury Deposition Network [*National Atmospheric Deposition Program*, 2003] to within 10%.

3.2. Ocean Mixed Layer Mercury Model

[15] The atmosphere-ocean exchange of mercury is determined by coupling GEOS-Chem with a slab model of the ocean mixed layer. The slab ocean has the same horizontal resolution as the atmospheric model, and each slab ocean box communicates with the atmospheric box directly above it. The ocean model contains three mercury tracers: Hg^0_{aq}, Hg^{II}_{aq}, and Hg^{nr}_{aq}, where Hg^{nr}_{aq} is the nonreactive fraction of the mercury pool, or the difference between total aqueous mercury (Hg^{tot}_{aq}) and the sum of $Hg^0_{aq} + Hg^{II}_{aq}$. We compare Hg^0_{aq} to observations of DGM, as $(CH_3)_2Hg$ concentrations are generally very low in surface waters [*Mason and Fitzgerald*, 1993; *Cossa et al.*, 1994]. We consider the sum of $Hg^0_{aq} + Hg^{II}_{aq}$ to be comparable to observations of reactive mercury, while Hg^{tot}_{aq} is compared to observations of total mercury. The slab ocean model neglects horizontal transport but takes into account vertical exchange.

[16] Within the slab ocean is a simplified representation of aqueous mercury processes, shown in Figure 2. Atmospheric Hg^{II} deposited to the ocean becomes Hg^{II}_{aq} and is either reduced to Hg^0_{aq} with rate constant k_p, or converted to Hg^{nr} with rate constant k_c. Hg^0_{aq} is lost to the atmosphere through a net sea-air flux (F_{oa}), while Hg^{nr} is lost to the

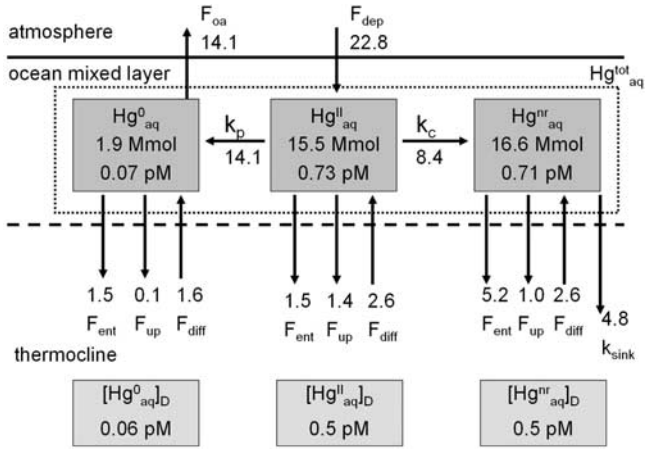

Figure 2. Annual global ocean budget of mercury for the standard simulation. F_{oa} is the sea-air flux, F_{dep} is deposition from the atmosphere, k_p is reduction of Hg^{II} to Hg^0, k_c is conversion of Hg^{II} to nonreactive forms, k_{sink} is particulate sinking, F^X_{up} is net upwelling of species X, F^X_{ent} is entrainment/detrainment of species X as the mixed layer depth changes, and F^X_{diff} is diffusion of species X from below. All fluxes are in Mmol yr^{-1}, tracer amounts are in Mmol, and concentrations are in pM.

deep ocean by particulate sinking with rate constant k_{sink}. All three aqueous species in the mixed layer are exchanged vertically with the deep ocean by upwelling (F_{up}) and diffusion across the thermocline (F_{diff}). In addition, when the mixed layer deepens or shoals, mercury from the deep ocean is entrained or detrained into the mixed layer (F_{ent}). Thus the mass balance equations for the three aqueous mercury species are

$$\frac{d\left[Hg^{II}_{aq}\right]}{dt} = \frac{F_{dep}}{z} - k_c\left[Hg^{II}_{aq}\right] - k_p\left[Hg^{II}_{aq}\right] + \frac{F^{II}_{ent} + F^{II}_{diff} + F^{II}_{up}}{z}, \quad (1)$$

$$\frac{d\left[Hg^{0}_{aq}\right]}{dt} = k_p\left[Hg^{II}_{aq}\right] + \frac{F^{0}_{ent} + F^{0}_{diff} + F^{0}_{up}}{z} - \frac{F_{oa}}{z}, \quad (2)$$

$$\frac{d\left[Hg^{nr}_{aq}\right]}{dt} = k_c\left[Hg^{II}_{aq}\right] + \frac{F^{nr}_{ent} + F^{nr}_{diff} + F^{nr}_{up}}{z} - k_{sink}\left[Hg^{nr}_{aq}\right]. \quad (3)$$

All concentrations ($[Hg^X_{aq}]$) are in moles m^{-3}, fluxes (F_i) are in moles m^{-2} s^{-1}, rate constants (k_j) are in s^{-1}, and the mixed layer depth (z) is in meters. Below we describe the parameterization of each term. In particular, the three rate constants (k_c, k_p, and k_{sink}) are expected to be highly variable and are poorly constrained. Our approach is to choose scaling factors for these rate constants in order to best reproduce mean observations of DGM, reactive mercury and total mercury.

[17] To account for both biological and photochemical reduction of Hg^{II}, we parameterize the reduction rate k_p as the product of local shortwave solar radiation at the ground (*RAD*, W m^{-2}), net primary productivity (*NPP*, gC m^{-2} $month^{-1}$), and a scaling parameter (α). We use *NPP* as a proxy for biological productivity because of its availability from satellite observations. We assume that reduction only occurs within the top 100 m of the mixed layer, the level at which light has attenuated to approximately 1% of its surface level,

$$k_p = \alpha \times NPP \times RAD \times \frac{\min(z, 100)}{z}. \quad (4)$$

[18] The scaling parameter α is set to 6.1×10^{-24} m^4 $month$ W^{-1} gC^{-1} s^{-1} to yield the best fit to aqueous observations (see above). Three-hour average values of *RAD* are taken from the GEOS-4 meteorological fields, while monthly average *NPP* fields are from the MODIS satellite [*Esaias*, 1996] for 2003 (http://eosdatainfo.gsfc.nasa.gov/eosdata/ssinc/amodoc_l4m_1d.shtml) and regridded to 4° × 5° resolution. The resulting global mean value for k_p is 2.4×10^{-8} s^{-1}. In biologically productive regions, it increases to 1.2×10^{-7} s^{-1}. Experiments in the open ocean report reduction rates of 2×10^{-8} s^{-1}–3.5×10^{-7} s^{-1} [*Mason et al.*, 1995, and references therein; *Lamborg et al.*, 1999]. Our values of k_p are thus on the same order of magnitude as these experiments. We have investigated alternative formulations of k_p (linear dependence on *NPP* and *RAD*, dependence on *RAD* only), but do not find significant differences in the spatial distribution of aqueous concentrations or in the predicted sea-air flux, except that reducing the dependence on *NPP* reduces the sea-air flux from productive high-latitude regions.

[19] We assume that conversion of Hg^{II}_{aq} to Hg^{nr}_{aq} is governed by the uptake of mercury on biologically derived particles with the rate constant k_c,

$$k_c = \gamma \times NPP. \quad (5)$$

Globally, the mean value of k_c is 1.7×10^{-8} s^{-1} (with the scaling factor, $\gamma = 6.9 \times 10^{-22}$ m^2 $month$ gC^{-1} s^{-1}).

[20] We describe the loss of Hg^{nr}_{aq} by particulate sinking, k_{sink}, based on estimates of the carbon flux. The carbon flux is determined by multiplying *NPP* by the temperature-dependent *ef* ratio, defined as the ratio of export production to total production, from *Laws et al.* [2000]. This approach yields a carbon export of 13 Gt $year^{-1}$, which is at the upper end of estimates ranging from 3.4 Gt $year^{-1}$ [*Eppley and Peterson*, 1979] to 13–15 Gt $year^{-1}$ [*Emerson*, 1997]. This flux is then multiplied by a scaling parameter ($\beta = 1.0 \times 10^{-21}$ m^2 $month$ gC^{-1} s^{-1}),

$$k_{sink} = \beta \times NPP \times ef. \quad (6)$$

The global mean value of k_{sink} is 9.3×10^{-9} s^{-1}. In productive regions, it increases to 3.4×10^{-8} s^{-1}.

[21] Air-sea exchange of elemental mercury is given by

$$F_{oa} = k_w \times \left(\left[Hg^0_{aq}\right] - H\left[Hg^0_{air}\right]\right), \quad (7)$$

where H is the dimensionless temperature-dependent Henry's Law constant [*Wängberg et al.*, 2001], and k_w is

the gas exchange velocity in m s^{-1}. The gas exchange velocity is taken from *Nightingale et al.* [2000], and adapted for mercury using the Schmidt numbers for CO_2 and Hg [*Poissant et al.*, 2000, and references therein], with the diffusivity for Hg from *Reid et al.* [1987].

[22] The monthly mixed layer depth, z, is from the Navy Mixed Layer Depth Climatology [*Kara et al.*, 2003] (http://www7320.nrlssc.navy.mil/nmld/nmld.html), which we regridded from $1^\circ \times 1^\circ$ to $4^\circ \times 5^\circ$ resolution. As the mixed layer deepens, all three species of aqueous mercury are entrained as follows:

$$F^X_{ent} = \frac{dz}{dt}\left(\left[Hg^X_{aq}\right]_D - \left[Hg^X_{aq}\right]\right), \quad (8)$$

where F^X_{ent} is the entrainment flux of species X (in moles m^{-2} $month^{-1}$) and $[Hg^X_{aq}]_D$ is the concentration in the deep ocean. When the mixed layer shoals (dz/dt < 0), mercury mass is lost so that mercury concentrations are conserved. The deep ocean concentrations are assumed to be constant with values of 0.06 pM, 0.5 pM, and 0.5 pM for Hg^0_{aq}, Hg^{II}_{aq}, and Hg^{nr}_{aq}, respectively. The Hg^0_{aq} deep concentration is assumed to be close to the mixed layer concentration as Hg^0_{aq} concentrations are nearly constant with depth [*Mason et al.*, 1998; *Ferrara et al.*, 2003]. $[Hg^{II}_{aq}]_D$ and $[Hg^{nr}_{aq}]_D$ are chosen at the lower end of observed depth profiles [*Mason and Fitzgerald*, 1993; *Mason et al.*, 1998, 2001; *Mason and Sullivan*, 1999; *Cossa et al.*, 2004; and *Laurier et al.*, 2004].

[23] We use monthly global wind stress data from *Hellerman and Rosenstein* [1983] to derive the upwelling velocity from Ekman pumping, W_e, which is the vertical velocity associated with divergence or convergence of water due to wind-driven currents. The net upwelling flux of species Hg^X_{aq} is described as

$$F^X_{up} = \max(W_e, 0)\left[Hg^X_{aq}\right]_D + \min(W_e, 0)\left[Hg^X_{aq}\right]. \quad (9)$$

[24] Finally, mercury can enter the mixed layer via diffusion from the thermocline [*Mason and Fitzgerald*, 1993],

$$F^X_{diff} = D_z \times \frac{\Delta\left[Hg^X_{aq}\right]_T}{\Delta h}, \quad (10)$$

where D_z is the thermocline diffusivity, taken to be 0.5 cm^2 s^{-1} (S. Emerson, personal communication, 2004). $\Delta[Hg^X_{aq}]_T/\Delta h$ is the concentration gradient with depth of species X at the top of the thermocline, which we assume to be 0.3 pM/100 m, 0.5 pM/100 m, and 0.5 pM/100 m for Hg^0_{aq}, Hg^{II}_{aq}, and Hg^{nr}_{aq}, respectively, on the basis of observed profiles [*Mason and Fitzgerald*, 1993]. Consequently, F_{diff} is a uniform, positive flux of mercury into the mixed layer.

[25] As the ocean mercury budget is poorly constrained in terms of observations and understanding of processes, our initial approach has been to use a simplified slab ocean model formulation. In doing so we have neglected a number of processes, which represent limitations in our model. First, the slab model ignores horizontal advection. The modeled lifetimes of Hg^{II}_{aq} and Hg^{nr}_{aq} in the ocean mixed layer range from weeks to years, long enough to allow oceanic advection. For characteristic ocean currents of 0.03–0.3 m/s, these species could be transported from one grid box to the next over their lifetime, or at the upper end of current speed, across an ocean basin. Lateral advection along isopycnals can affect the latitudinal distribution of Hg when isopycnal surfaces from high Hg deposition areas outcrop at higher latitudes [*Laurier et al.*, 2004]. Ocean advection would thus act to smooth out the model calculated distributions of Hg^{II}_{aq} and Hg^{nr}_{aq}. The assumption of globally uniform values for the concentrations and gradients of mercury below the mixed layer is also a simplification, as observations indicate differences in the Atlantic and Pacific deep ocean Hg concentrations [*Cossa et al.*, 2004; *Mason et al.*, 1998; *Gill and Fitzgerald*, 1988; *Laurier et al.*, 2004]. Additionally, the description of aqueous mercury chemistry in the model is very simple, and we do not explicitly account for methylated, particulate, and colloidally bound forms of mercury. The reduction of Hg^{II}_{aq} to Hg^0_{aq} is treated as a one-way net process, whereas observations suggest that the reverse reaction, oxidation of Hg^0_{aq}, may also occur [*Amyot et al.*, 1997, *Lalonde et al.*, 2001; *Mason et al.*, 2001].

4. Results

4.1. Global Ocean Budget

[26] Figure 2 summarizes the global ocean budget of mercury in our simulation. The mean global oceanic concentrations of Hg^0_{aq}, Hg^{II}_{aq}, and Hg^{nr}_{aq} in the model's mixed layer are 0.07, 0.73, and 0.71 pM, respectively, with corresponding burdens of 1.9, 15.5, and 16.6 Mmol. Mercury enters the ocean mixed layer primarily through deposition of Hg^{II} (22.8 Mmol yr^{-1}), with an additional 6.8 Mmol yr^{-1} from diffusion from the thermocline. The sources to the ocean are balanced by a loss of Hg^0 to the atmosphere (14.1 Mmol yr^{-1}), exchange with the deep ocean (10.7 Mmol yr^{-1}) and particulate sinking of Hg^{nr}_{aq} (4.8 Mmol yr^{-1}).

[27] Atmospheric deposition and conversion of Hg^{II}_{aq} to Hg^0_{aq} and Hg^{nr}_{aq} control the levels of Hg^{II}_{aq}. The resulting global mean lifetime of Hg^{II}_{aq} is 7.3 months. Most of the Hg^0_{aq} is then lost through evasion to the atmosphere with a global mean lifetime of 1.5 months. Hg^{nr}_{aq} has a mixed layer source from conversion of Hg^{II}_{aq}, as well as diffusion. These sources are balanced by losses through mixing and particulate sinking, resulting in a 1.5 year lifetime.

[28] Table 1 summarizes our mixed layer mercury ocean budget and compares it to previous studies based on box models of the ocean [*Mason et al.*, 1994a; *Mason and Sheu*, 2002; *Lamborg et al.*, 2002]. The apparent discrepancy in the burdens of mercury for all these studies results from the use of different mixed layer depths. Normalizing all the results to a 100 m mixed layer, we have a burden of 64 Mmol, which is consistent with the other estimates (54–72 Mmol).

[29] Our net ocean-atmosphere flux of 14.1 Mmol yr^{-1} is at the upper end of these previous estimates (4–13 Mmol yr^{-1}, Table 1). As noted in section 3.2, the rate constants in our model are adjusted in order to reproduce observed mean

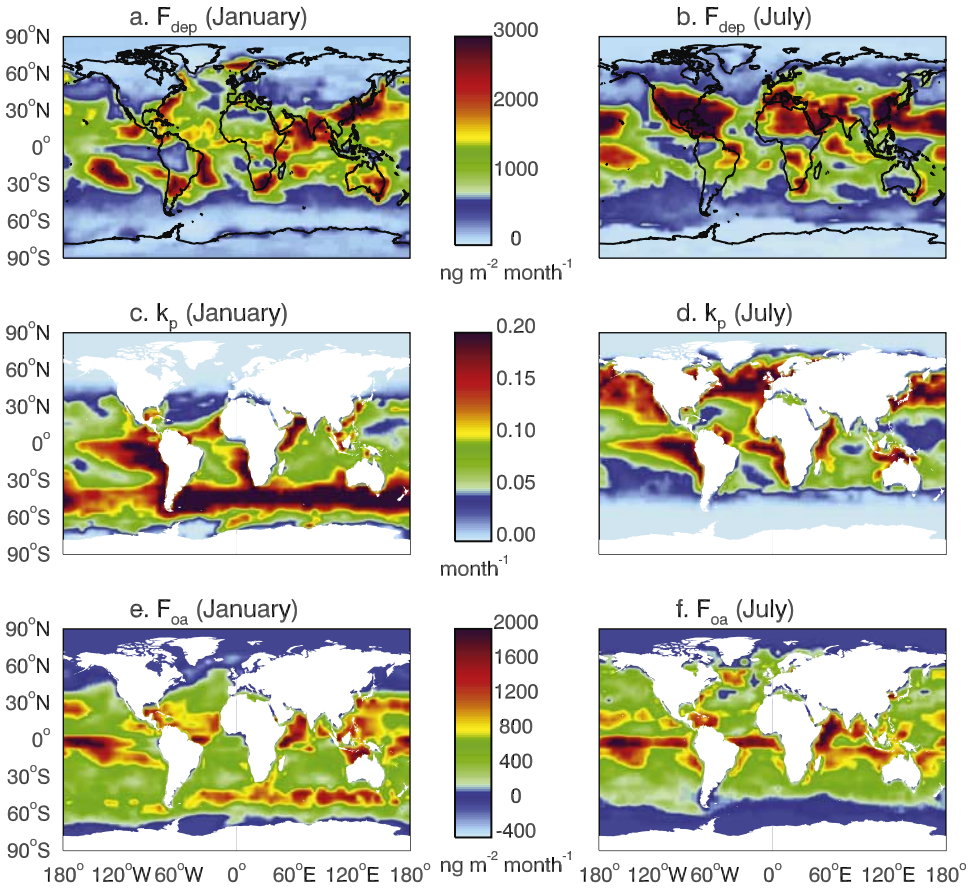

Figure 3. (a, b) Monthly mean mercury deposition (wet + dry) flux; (c, d) reduction rate constant, k_P; and (e, f) ocean flux F_{oa} for January and July. Positive values of F_{oa} indicate that the flux is from the ocean to the atmosphere.

aqueous concentrations. Thus our ocean-atmosphere flux is constrained by observations of aqueous mercury, in particular elemental mercury (see section 4.3). Deposition provides 90% of the mixed layer Hg^{II}_{aq}, resulting in reduction of 12.7 Mmol yr^{-1} of recently deposited mercury to Hg^{0}_{aq}. Thus 89% of the mixed layer Hg^{0}_{aq}, and hence of the ocean source, originates from recently deposited mercury, while the remaining 11% comes from below the mixed layer.

[30] Our deposition source to the ocean (22.8 Mmol yr^{-1}) is larger than previous estimates (10–15.4 Mmol yr^{-1}, Table 1). Our global deposition (33.9 Mmol yr^{-1}) is similar to that of *Mason and Sheu* [2002] (33 Mmol yr^{-1}), but we find a larger fraction of deposition to the ocean (67%) compared to their 47%. *Lamborg et al.* [2002] assume that 48% of their global deposition occurs over oceans, but they have a smaller global sink of mercury by deposition (21 Mmol yr^{-1}) because their land and ocean emissions are smaller. Our large deposition to the ocean results from the high dry deposition velocity for Hg^{II} needed to reproduce observations of RGM in the boundary layer. Our assumed rapid uptake of RGM on sea-salt aerosols followed by dry deposition further contributes to our elevated oceanic deposition (see *Selin et al.* [2007] for a detailed discussion).

[31] Because of this large deposition source, mass balance requires GEOS-Chem to have a larger net loss to the deep ocean: 8.7 Mmol yr^{-1} as compared to 6 Mmol yr^{-1} given by *Lamborg et al.* [2002] and 3.4 Mmol yr^{-1} given by *Mason and Sheu* [2002]. Considering only particulate sinking from the mixed layer, our model has a loss of 4.8 Mmol yr^{-1}, in between the 9 Mmol yr^{-1} estimate of *Lamborg et al.* [2002] and the 1.4 Mmol yr^{-1} estimate of *Mason and Sheu* [2002]. The partitioning of loss to the deep ocean between particulate sinking and vertical mixing is sensitive to our choice of deep ocean mercury concentrations. If we triple the deep concentrations of Hg^{II}_{aq} and Hg^{nr}_{aq}, we find that particulate sinking represents 52% of the loss to the deep ocean where as it was only 31% in the standard simulation. Loss from the deep ocean by sediment burial is constrained by the sedimentary record at 1 Mmol yr^{-1} [*Mason and Fitzgerald*, 1996]. Thus our net accumulation of mercury in the deep ocean is 7.7 Mmol yr^{-1}, implying an ~0.7%/yr increase in deep ocean mercury concentrations, nearly 4 times larger than the estimate of *Mason and Sheu* [2002] and 75% larger than the estimated rate of increase in the thermocline [*Lamborg et al.*, 2002].

4.2. Global Distributions

[32] The global distribution of aqueous mercury species is determined primarily by the global patterns of deposition; primary productivity, which affects the conversion of Hg^{II}_{aq} to Hg^{0}_{aq} and Hg^{nr}_{aq} and determines the loss of Hg^{nr}_{aq}; and upwelling (Figures 3 and 4) (S. Emerson, personal commu-

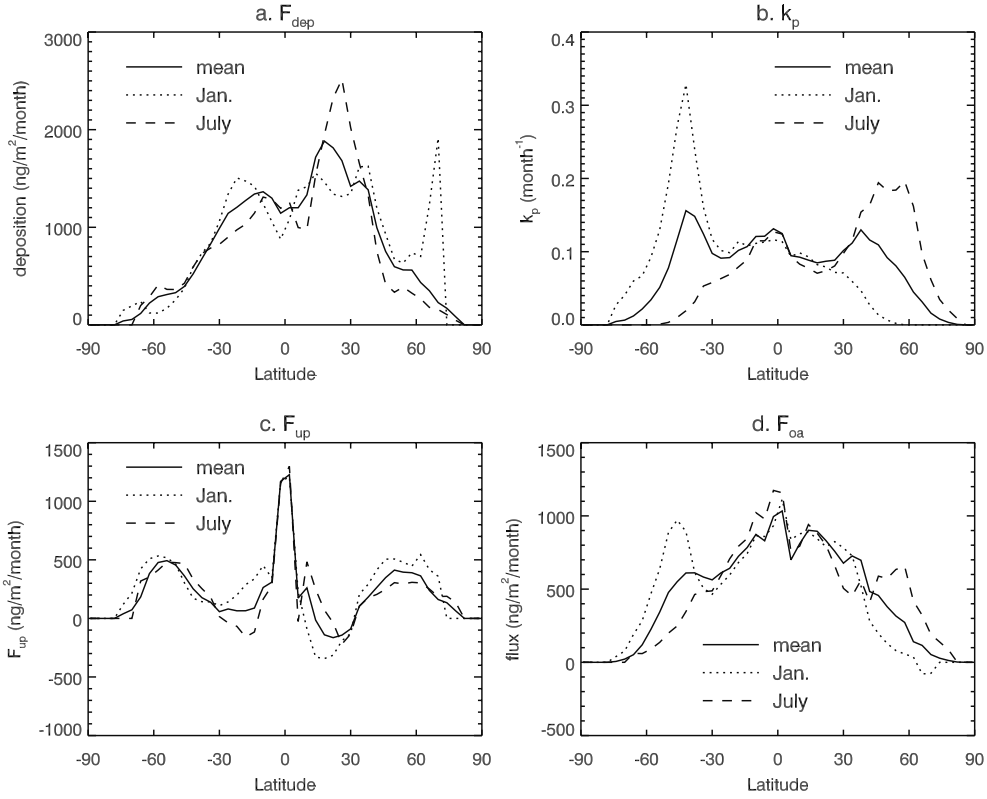

Figure 4. Latitudinal distribution of (a) atmospheric deposition to the ocean, F_{dep}, (b) Hg_{aq}^{II} to Hg_{aq}^{0} reduction rate, k_p, (c) upwelling flux of total mercury, F_{up}, and (d) ocean flux, F_{oa}, in January and July, as well as the annual mean.

nication, 2004). The model shows high mercury deposition in the tropics because of high precipitation plus rapid atmospheric oxidation rates producing RGM for dry deposition. Deposition is also high in the western North Atlantic and western North Pacific, which are downwind of large industrial regions of the eastern U.S. and East Asia (Figures 3a and 3b).

[33] Because of its dependence on *NPP*, the reduction rate constant k_p is largest in the productive upwelling regions, while the ocean gyres have low reduction rates (Figures 3c, 3d, and 4b), consistent with the observations of *Kim and Fitzgerald* [1986]. Seasonally, high production regions migrate from the Southern Hemisphere (SH) in January to the Northern Hemisphere (NH) in July (Figures 3c, 3d, and 4b). High reduction rates also occur in coastal upwelling regions such as the west coast of Peru. The most prominent features in the spatial distribution of F_{up} are strong upwelling at the equator and downwelling in the subtropics (Figure 4c).

[34] Figure 5 (top) shows the modeled annual reactive (Hg_{aq}^{II} + Hg_{aq}^{0}) and total (Hg_{aq}^{tot}) mercury concentrations in the surface ocean. The model displays high concentrations of both reactive and total mercury (>1.5 pM) in the tropics, due to large upwelling and deposition fluxes (Figures 4a and 4c). Reactive and total mercury concentrations are also enhanced off the east coasts of the United States and East Asia because of large atmospheric deposition fluxes (Figures 3a and 3b). Figure 5 (bottom) shows the modeled Hg_{aq}^{0} concentrations in June–August and December–February. In tropical regions, high values of upwelling, deposition, and productivity are colocated, providing Hg_{aq}^{II} that is then quickly reduced to Hg_{aq}^{0}. This results in large Hg_{aq}^{0} concentrations along the equator (0.01–0.66 pM) in all seasons. Concentrations of Hg_{aq}^{0} are also elevated at high latitudes during summer (>0.15 pM) because of high biological activity and thus enhanced reduction of deposited mercury (Figures 3 and 4).

4.3. Comparison to Observed Aqueous Mercury Concentrations

[35] The observations (Figure 5 and auxiliary material Tables S2 and S3), like the model, show higher concentrations of Hg_{aq}^{II} + Hg_{aq}^{0} and Hg_{aq}^{tot} in regions of high deposition (downwind of Asia and the United States), as well as in regions with high biological productivity and upwelling (Equator, high latitudes during summer, and on the west coast of Peru). As discussed in section 3.2, we have chosen our scaling parameters α, β and γ to match the mean observations of aqueous elemental, reactive and total mercury. We have done so by minimizing the mean model bias: (model-observations)/observations for regions where data is available. However, the model does not capture the full range of variability found in the observations. For 88% of the reactive mercury observations, the model is within 60%

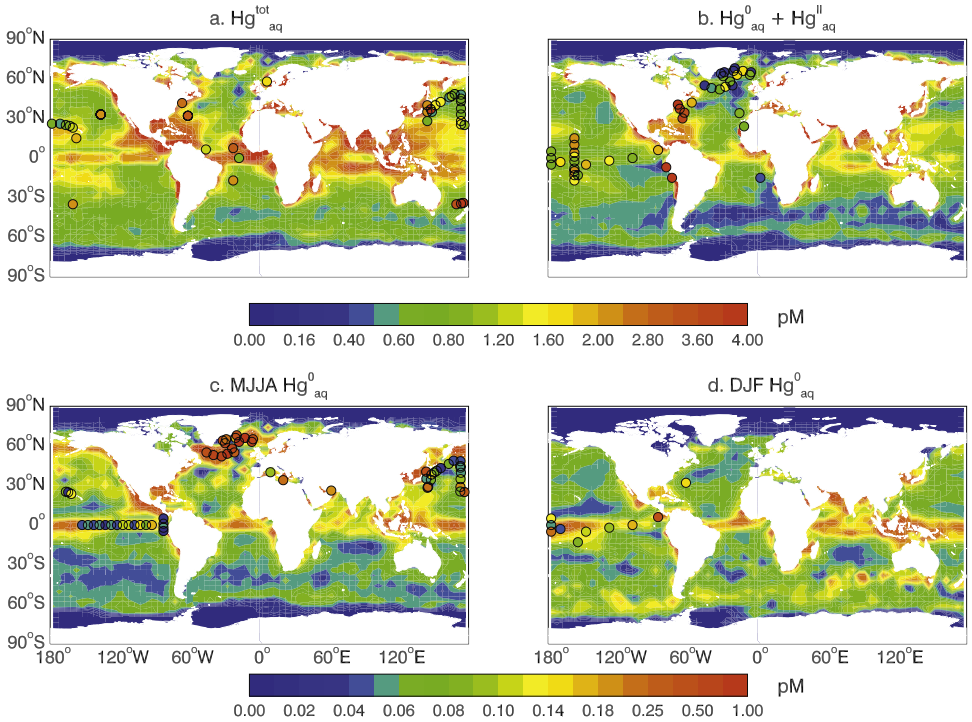

Figure 5. Modeled concentrations of annual average total (a) aqueous mercury and (b) reactive mercury in pM. Observations from *Coquery and Cossa* [1995], *Dalziel* [1992, 1995], *Gill and Fitzgerald* [1987], *Mason et al.* [2001], *Mason and Sullivan* [1999], and *Laurier et al.* [2004] are overplotted in circles. Modeled elemental mercury concentrations for (c) May–August and (d) December–February. The circles are observations from *Gårdfeldt et al.* [2003], *Kim and Fitzgerald* [1986], *Mason and Fitzgerald* [1993], *Mason et al.* [1998], *Mason et al.* [2001], and F. Laurier (personal communication, 2005).

of the observations, while for Hg^{tot}_{aq} the model is within ±100% of the observations (auxiliary material Tables S2 and S3). Modeled Hg^{0}_{aq} also displays less variability than the observations (Table S1 in auxiliary materials and Figures 5c and 5d). In particular, concentrations in August in the North Atlantic are underestimated by a factor of 3. However, these observations are high (0.3–0.53 pM) compared to many of the others (0.05–0.12 pM), and could represent a temporary situation in which Hg^{0}_{aq} has been produced faster than it can be removed [*Mason et al.*, 1998].

[36] Some of the variability in observations could be due to local stratification in the mixed layer, which cannot be captured by the model. Indeed, observations show that mercury concentrations can vary with depth in the mixed layer by a factor of 3 or more [e.g., *Mason and Fitzgerald*, 1993; *Dalziel*, 1995].

4.4. Ocean-Atmosphere Flux

[37] The ocean-atmosphere flux, F_{oa}, depends on Hg^{0}_{aq} concentrations as well as on temperature, via the Henry's law constant and k_w, and wind speed, via k_w (see equation (7)). The largest fluxes occur in the tropical regions and low fluxes toward the midlatitudes, with the annual mean decreasing from 1000 ng m^{-2} month^{-1} to 600 ng m^{-2} month^{-1} between the equator and 40° (Figure 4d). This agrees with evasion flux estimates over the equatorial and North Pacific showing higher evasion in the tropics compared to northern waters [*Kim and Fitzgerald*, 1986; *Laurier et al.*, 2003]. In tropical regions, high Hg^{0}_{aq} concentrations together with warm temperatures cause a greater degree of supersaturation, which results in a strong evasion flux to the atmosphere. F_{oa} displays large seasonal variability poleward of 30° latitude (Figures 3e, 3f, and 4d). Strong positive F_{oa} values are present near 50°S in January and 60°N in July, due to the high level of biological activity and thus elevated Hg^{0}_{aq} (Figures 3c, 3d, and 4d). At high latitudes of the winter hemisphere, the ocean is a net sink for Hg^0 ($F_{oa} < 0$) as a result of cold water temperatures causing the ocean to be undersaturated in Hg^0. This is consistent with the finding of *Marks and Beldowska* [2001] that the Baltic Sea experiences an air-sea transport of mercury during the winter.

[38] We examined the sensitivity of F_{oa} to the formulation of k_w. If we use the parameterization of *Liss and Merlivat* [1986], we find that for the same DGM concentrations the model calculates a sea-air flux of 10.2 Mmol/yr, a 28% reduction over our standard simulation using *Nightingale et al.* [2000].

4.5. Contribution of Ocean Emissions to Atmospheric Mercury

[39] We compare cruise observations of atmospheric TGM over the Atlantic [*Temme et al.*, 2003; *Slemr*, 1996] with our model simulation in Figure 6. The model system-

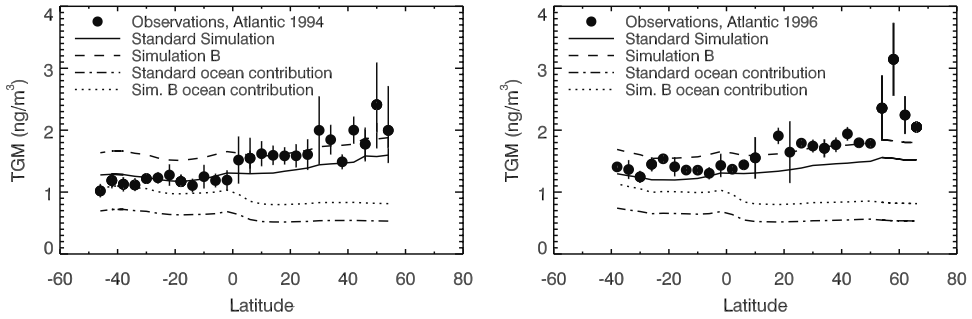

Figure 6. Observed atmospheric TGM concentrations over the Atlantic Ocean in (left) 1994 [*Slemr*, 1996] and (right) 1996 [*Temme et al.*, 2003] are shown in black circles. The observations are averaged by model grid box, and the error bars represent the standard deviation of the observations within a grid box. Model results sampled along the cruise track for the standard simulation (solid line) and a simulation with a 21.7 Mmol yr^{-1} ocean flux (simulation B, dashed line) are also shown. The dash-dotted and dotted lines represent the ocean contribution to the surface atmospheric concentration for the standard simulation and simulation B, respectively.

atically underestimates observations in the NH by 25% and has an interhemispheric gradient of 1.2, smaller than the observed gradient of 1.5. *Selin et al.* [2007] demonstrates that the GEOS-Chem model does reproduce land-based observations, which are lower than the ocean cruise observations at the same latitude [*Selin et al.*, 2007, Figure 3]. Increasing ocean emissions from 14.1 Mmol yr^{-1} to 21.7 Mmol yr^{-1} (simulation B) results in better agreement with the cruise observations in the NH (dashed line in Figure 6), but systematically overestimates SH cruise observations as well as land-based observations (not shown). Thus the magnitude of the ocean emissions cannot resolve this discrepancy between model and cruise observations. One possibility is that halogen chemistry in the marine boundary layer, which the model neglects, could shift the latitudinal distribution of deposition to the ocean and hence of the ocean flux. Another possibility is that biomass burning emissions, currently neglected in the model, could provide another NH and tropical source.

[40] The contribution of ocean emissions to surface atmospheric Hg^0 concentrations is shown in Figure 7, which was obtained by comparing our standard simulation to a simulation without ocean emissions. In the SH, where anthropogenic and land sources are relatively small, ocean emissions account for 54% of surface atmospheric mercury, while in the NH, their contribution is 36% on average. As expected, the ocean plays a smaller role (<30%) over regions with large anthropogenic sources.

[41] The seasonal cycle of regional ocean emissions and their contribution to surface atmospheric Hg^0 concentrations is shown in Figure 8. Ocean emissions at midlatitudes over the northern Pacific and Atlantic increase by a factor of 2 between winter and spring. This rapid spring increase, which reaches a maximum in May–June, is driven by the increase in biological productivity and thus large production of Hg^0_{aq} via reduction of Hg^{II}_{aq}. This is further enhanced by a decrease in mixed layer depth during that period, leading to the accumulation of atmospheric deposition in a smaller volume and thus larger Hg^0_{aq} concentrations.

[42] The maximum effect of ocean emissions on atmospheric concentrations occurs in June in the NH and December in the SH. The largest seasonal cycles (defined as maximum/minimum) in background Hg^0 originating from the ocean are seen over the North pacific (1.32), North Atlantic (1.24), and Europe (1.28). This seasonal cycle is smaller over North America (1.21) and the South Pacific (1.15).

5. Summary

[43] We have coupled a global atmospheric model of mercury transport with an interactive slab model of the ocean mixed layer to constrain estimates of ocean emissions, simulate their spatiotemporal variability, and examine the role of the ocean in mercury cycling. We use observations of aqueous elemental (Hg^0_{aq}), reactive (Hg^0_{aq} + Hg^{II}_{aq}), and total mercury (Hg^{tot}_{aq} = Hg^0_{aq}+Hg^{II}_{aq}+Hg^{nr}_{aq}) to constrain our oceanic simulation.

[44] Our modeled mixed layer budget shows mercury entering the ocean mixed layer primarily through atmo-

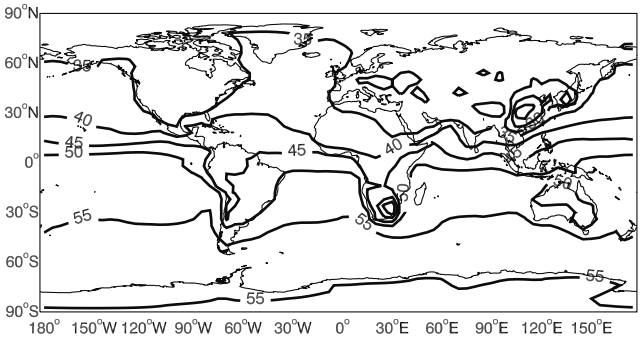

Figure 7. Percent contribution of ocean emissions to atmospheric surface concentrations of Hg^0. Contours shown are between 25% and 55%, with increments of 5%.

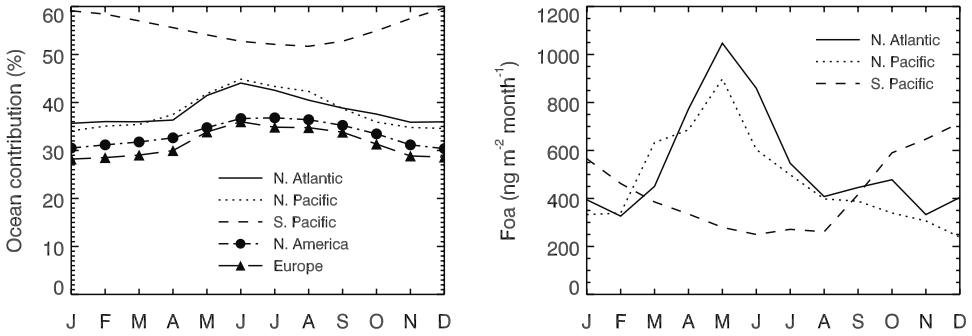

Figure 8. (left) Seasonal variation in the contribution of the ocean source to surface concentrations of Hg^0 in the North Atlantic (48°W–12°W, 30°N–60°N; solid line), North Pacific (180°W–138°W, 30°N–60°N; dotted line), South Pacific (180°W–78°W, 30°S–60°N; dashed line), Europe (5°W–45°E, 42°N–74°N; triangles), and North America (50°W–162°W, 18°N–74°N; circles). (right) Seasonal variation in F_{oa} for the North Atlantic, North Pacific, and South Pacific.

spheric deposition of Hg^{II} (22.8 Mmol yr^{-1}), with a smaller contribution from diffusion across the thermocline (6.8 Mmol yr^{-1}). Within the mixed layer, 33% of Hg^{II}_{aq} is converted to Hg^{nr}_{aq}, while 56% is reduced to Hg^0_{aq} and lost to the atmosphere and the remaining 11% is lost through mixing to the deep ocean.

[45] The resulting aqueous concentrations of mercury in the surface ocean are 0.07 pM, 0.73 pM, and 0.71 pM for Hg^0_{aq}, Hg^{II}_{aq}, and Hg^{nr}_{aq}, respectively, consistent with observed values. The modeled concentrations display the same spatial and temporal features as the observations but do not reproduce the full range of variability observed. Concentrations of total and reactive aqueous mercury are high year round in tropical regions where high deposition and strong upwelling coincide. Hg^0_{aq} concentrations are elevated in upwelling regions and show seasonal variability with high concentrations occurring in the northern and southern oceans during times of intense biological productivity.

[46] We find a net global ocean evasion flux of 14.1 Mmol yr^{-1}, at the upper end of previous estimates (4–13 Mmol yr^{-1}). Re-emission of previously deposited mercury accounts for 89% of our ocean emissions, the remaining fraction coming from evasion of deep ocean mercury transported to the surface. The modeled ocean emissions are enhanced in the tropics for all seasons owing to high deposition, upwelling, and warm temperatures. A secondary maximum in ocean emissions occurs at mid and high latitudes during late spring to early summer coincident with high biological productivity in these regions.

[47] Mass balance requires GEOS-Chem to have an 8.7 Mmol yr^{-1} net loss to the deep ocean, larger than previous estimates (3.4–6 Mmol yr^{-1}). Our coupled ocean-atmosphere simulation thus implies that the deep ocean acts as a dominant sink of mercury, with concentrations increasing at a rate of ~0.7%/yr.

[48] We find that ocean evasion is a major contributor to atmospheric concentrations of elemental mercury, particularly in the SH. The ocean contributes 36% of the NH and 54% of the SH surface atmospheric concentration, with the largest contribution occurring during summer.

[49] To improve our understanding of the spatial and seasonal variability of the ocean mercury source, as well as its overall magnitude, more measurements are needed in the open ocean. Measurements of speciated aqueous mercury in regions such as the southern Pacific and Indian oceans would be particularly useful. In addition, monthly measurements over regions with expected high seasonal variability, such as the North Atlantic, North Pacific, and Southern Ocean, would help elucidate the factors controlling the strong seasonality of ocean emissions.

[50] **Acknowledgments.** This work was supported by funding from the National Science Foundation under grant ATM 0238530. The GEOS-CHEM model is managed by the Atmospheric Chemistry Modeling group at Harvard University with support from the NASA Atmospheric Chemistry Modeling and Analysis Program. The authors wish to thank Steven Emerson for useful conversations.

References

Amyot, M., G. A. Gill, and F. M. M. Morel (1997), Production and loss of dissolved gaseous mercury in coastal seawater, *Environ. Sci. Technol.*, *31*, 3606–3611.

Bergan, T., and H. Rodhe (2001), Oxidation of elemental mercury in the atmosphere: Constraints imposed by global scale modeling, *J. Atmos. Chem.*, *40*, 191–212.

Bergan, T., L. Gallardo, and H. Rodhe (1999), Mercury in the global troposphere: A three dimensional model study, *Atmos. Environ.*, *33*, 1575–1585.

Bey, I., D. J. Jacob, R. M. Yantosca, J. A. Logan, B. Field, A. M. Fiore, Q. Li, H. Y. Liu, L. J. Mickley, and M. G. Schultz (2001), Global modeling of tropospheric chemistry with assimilated meteorology: Model description and evaluation, *J. Geophys. Res.*, *106*, 23,073–23,095.

Coquery, M., and D. Cossa (1995), Mercury speciation in surface waters of the North Sea, *Neth. J. Sea Res.*, *34*, 245–257.

Cossa, D., J.-M. Martin, and J. Sanjuan (1994), Dimethylmercury formation in the Alboran Sea, *Mar. Pollut. Bull.*, *28*, 381–384.

Cossa, D., M.-H. Cotté-Krief, R. P. Mason, and J. Bretaudeau-Sanjuan (2004), Total mercury in the water column near the shelf edge of the European continental margin, *Mar. Chem.*, *90*, 21–29.

Costa, M., and P. S. Liss (1999), Photoreduction of mercury in sea water and its possible implications for Hg^0 air-sea fluxes, *Mar. Chem.*, *68*, 87–95.

Dalziel, J. A. (1992), Reactive mercury on the Scotian Shelf and in the adjacent northwest Atlantic Ocean, *Mar. Chem.*, *37*, 171–178.

Dalziel, J. A. (1995), Reactive mercury in the eastern North Atlantic and southeast Atlantic, *Mar. Chem.*, *49*, 307–314.

Dastoor, A. P., and Y. Larocque (2004), Global circulation of atmospheric mercury: A modeling study, *Atmos. Environ.*, *38*, 147–161.

Emerson, S. (1997), Net biological oxygen production: A global estimate from oceanic measurements, in *Biogeochemical Processes in the North Pacific*, edited by S. Tunogai, pp. 143–155, Jpn. Mar. Sci. Found., Tokyo.

Eppley, R. W., and B. J. Peterson (1979), Particulate organic matter flux and planktonic new production in the deep ocean, *Nature*, *282*, 677–680.
Esaias, W. E. (1996), Algorithm theoretical basis document for MODIS product MOD-27 ocean primary productivity, report, NASA Goddard Space Flight Cent., Greenbelt, Md.
Ferrara, R., C. Ceccarini, E. Lanzillotta, K. Gårdfeldt, J. Sommar, M. Horvat, M. Logar, V. Fajon, and J. Kotnik (2003), Profiles of dissolved gaseous mercury concentration in the Mediterranean seawater, *Atmos. Environ.*, *37*, S85–S92.
Fitzgerald, W. F. (1986), Cycling of mercury between the atmosphere and oceans, in Role of Air-Sea Exchange in Geochemical Cycling, *NATO ASI Ser.*, vol. C185, pp. 363–408, Springer, New York.
Fitzgerald, W. F., D. R. Engstrom, R. P. Mason, and E. A. Nater (1998), The case for atmospheric mercury contamination in remote areas, *Environ. Sci. Technol.*, *32*, 1–7.
Gårdfeldt, K., et al. (2003), Evasion of mercury from coastal and open waters of the Atlantic Ocean and the Mediterranean Sea, *Atmos. Environ.*, *37*, S73–S84.
Gill, G. A., and W. F. Fitzgerald (1987), Mercury in surface waters of the open ocean, *Global Biogeochem. Cycles*, *1*, 199–212.
Gill, G. A., and W. F. Fitzgerald (1988), Vertical mercury distributions in the oceans, *Geochim. Cosmochim. Acta*, *52*, 1719–1728.
Guentzel, J. L., R. T. Powell, W. M. Landing, and R. P. Mason (1996), Mercury associated with colloidal material in an estuarine and an open-ocean environment, *Mar. Chem.*, *55*, 177–188.
Hall, B. (1995), The gas phase oxidation of elemental mercury by ozone, *Water Air Soil Pollut.*, *80*, 301–315.
Hedgecock, I. M., and N. Pirrone (2001), Mercury and photochemistry in the marine boundary layer-modelling studies suggest the in situ production of reactive gas phase mercury, *Atmos. Environ.*, *35*, 3055–3062.
Hedgecock, I. M., and N. Pirrone (2004), Chasing quicksilver: Modeling the atmospheric lifetime of $Hg^0_{(g)}$ in the marine boundary layer at various latitudes, *Environ. Sci. Technol.*, *38*, 69–76.
Hellerman, S., and M. Rosenstein (1983), Normal monthly wind stress over the world ocean with error estimates, *J. Phys. Oceanogr.*, *13*, 1093–1104.
Horvat, M., J. Kotnik, M. Logar, V. Fajon, T. Zvonarić, and N. Pirrone (2003), Speciation of mercury in surface and deep-sea waters in the Mediterranean Sea, *Atmos. Environ.*, *37*, S93–S108.
Hudson, R. J. M., S. A. Gherini, W. F. Fitzgerald, and D. B. Porcella (1995), Anthropogenic influences on the global mercury cycle: A model-based approach, *Water Air Soil Pollut.*, *80*, 265–272.
Kara, A. B., P. A. Rochford, and H. E. Hurlburt (2003), Mixed layer depth variability over the global ocean, *J. Geophys. Res.*, *108*(C3), 3079, doi:10.1029/2000JC000736.
Kim, J. P., and W. F. Fitzgerald (1986), Sea-air partitioning of mercury in the equatorial Pacific Ocean, *Science*, *231*, 1131–1133.
Lalonde, J. D., M. Amyot, A. M. L. Kraepiel, and F. M. M. Morel (2001), Photooxidation of Hg(0) in artificial and natural waters, *Environ. Sci. Technol.*, *35*, 1367–1372.
Lamborg, C. H., K. R. Rolfhus, W. F. Fitzgerald, and G. Kim (1999), The atmospheric cycling and air-sea exchange of mercury species in the South and equatorial Atlantic Ocean, *Deep Sea Res., Part II*, *46*, 957–977.
Lamborg, C. H., W. F. Fitzgerald, J. O'Donnell, and T. Torgersen (2002), A non-steady-state compartmental model of global-scale mercury biogeochemistry with interhemispheric atmospheric gradients, *Geochim. Cosmochim. Acta*, *66*, 1105–1118.
Lamborg, C. H., C.-M. Tseng, W. F. Fitzgerald, P. H. Balcom, and C. R. Hammerschidt (2003), Determination of the mercury complexation characteristics of dissolved organic matter in natural waters with "Reducible Hg" titrations, *Environ. Sci. Technol.*, *37*, 3316–3322.
Laurier, F. J. G., R. P. Mason, and L. Whalin (2003), Reactive gaseous mercury formation in the North Pacific Ocean's marine boundary layer: A potential role of halogen chemistry, *J. Geophys. Res.*, *108*(D17), 4529, doi:10.1029/2003JD003625.
Laurier, F. J. G., R. P. Mason, G. A. Gill, and L. Whalin (2004), Mercury distributions in the North Pacific Ocean—20 years of observations, *Mar. Chem.*, *90*, 3–19.
Laws, W. A., P. G. Falkowski, W. O. Smith Jr., H. Ducklow, and J. J. McCarthy (2000), Temperature effects on export production in the open ocean, *Global Biogeochem. Cycles*, *14*, 1231–1246.
Lindqvist, O., K. Johansson, M. Aastrup, A. Andersson, L. Bringmark, G. Hovsenius, L. Håkanson, Å. Iverfeldt, M. Meili, and B. Timm (1991), Mercury in the Swedish environment—Recent research on causes, consequences and corrective methods, *Water Air Soil Pollut.*, *55*, 11–13.
Liss, P. S., and L. Merlivat (1986), Air-sea gas exchange rates: Introduction and synthesis, in *The Role of Air-Sea Exchange in Geochemical Cycling*, edited by P. Buat-Ménard, pp. 113–127, Springer, New York.
Marks, R., and M. Beldowska (2001), Air-sea exchange of mercury vapour over the Gulf of Gdañsk and southern Baltic Sea, *J. Mar. Syst.*, *27*, 315–324.
Mason, R. P., and W. F. Fitzgerald (1993), The distribution and biogeochemical cycling of mercury in the equatorial Pacific Ocean, *Deep Sea Res., Part I*, *40*, 1897–1924.
Mason, R. P., and W. F. Fitzgerald (1996), Sources, sinks and biogeochemical cycling of mercury in the ocean, in *Global and Regional Mercury Cycles: Sources, Fluxes and Mass Balances*, edited by W. Baeyens et al., pp. 249–272, Elsevier, New York.
Mason, R. P., and G.-R. Sheu (2002), Role of the ocean in the global mercury cycle, *Global Biogeochem. Cycles*, *16*(4), 1093, doi:10.1029/2001GB001440.
Mason, R. P., and K. A. Sullivan (1999), The distribution and speciation of mercury in the South and equatorial Atlantic, *Deep Sea Res., Part II*, *46*, 937–956.
Mason, R. P., W. F. Fitzgerald, and F. M. M. Morel (1994a), The biogeochemical cycling of elemental mercury: Anthropogenic influences, *Geochim. Cosmochim. Acta*, *58*, 3191–3198.
Mason, R. P., J. O'Donnell, and W. F. Fitzgerald (1994b), Elemental mercury cycling within the mixed layer of the Equatorial Pacific Ocean, in *Mercury as a Global Pollutant: Towards Integration and Synthesis*, edited by C. J. Watras and J. W. Huckabee, pp. 83–97, CRC Press, Boca Raton, Fla.
Mason, R. P., F. M. M. Morel, and H. F. Hemond (1995), The role of microorganisms in elemental mercury formation in natural waters, *Water Air Soil Pollut.*, *80*, 775–787.
Mason, R. P., K. R. Rolfhus, and W. F. Fitzgerald (1998), Mercury in the North Atlantic, *Mar. Chem.*, *61*, 37–53.
Mason, R. P., N. M. Lawson, and G.-R. Sheu (2001), Mercury in the Atlantic Ocean: Factors controlling air-sea exchange of mercury and its distribution in the upper waters, *Deep Sea Res., Part II*, *48*, 2829–2853.
Morel, F. M. M., A. M. L. Krapiel, and M. Amyot (1998), The chemical cycle and bioaccumulation of mercury, *Annu. Rev. Ecol. Syst.*, *29*, 543–566.
National Atmospheric Deposition Program (2003), Mercury Deposition Network (MDN): A NADP Network, NADP Program Off., Ill. State Water Surv., Champaign.
National Research Council (2000), *Toxicological Effects of Methylmercury*, Natl. Acad., Washington, D. C.
Nightingale, P. D., G. Malin, C. S. Law, A. J. Watson, P. S. Liss, M. I. Liddicoat, J. Boutin, and R. C. Upstill-Goddard (2000), In situ evaluation of air-sea gas exchange parameterizations using novel conservative and volatile tracers, *Global Biogeochem. Cycles*, *14*, 373–387.
Pacyna, J. M., E. G. Pacyna, F. Steenhuisen, and S. Wilson (2003), Mapping 1995 global anthropogenic emissions of mercury, *Atmos. Environ.*, *37*, S109–S117.
Poissant, L., M. Amyot, M. Pilote, and D. Lean (2000), Mercury water-air exchange over the Upper St. Lawrence River and Lake Ontario, *Environ. Sci. Technol.*, *34*, 3069–3078.
Reid, R. C., J. M. Prausnitz, and B. E. Poling (1987), *The Properties of Gases and Liquids*, McGraw-Hill Inc., New York.
Rolfhus, K. R., and W. F. Fitzgerald (2004), Mechanisms and temporal variability of dissolved gaseous mercury production in coastal seawater, *Mar. Chem.*, *90*, 126–136.
Schroeder, W. H., and J. Munthe (1998), Atmospheric mercury—An overview, *Atmos. Environ.*, *32*, 809–822.
Seigneur, C., P. Karamchandani, K. Lohman, and K. Vijayaraghavan (2001), Multiscale modeling of the atmospheric fate and transport of mercury, *J. Geophys. Res.*, *106*, 27,795–27,809.
Seigneur, C., K. Vijayaraghavan, K. Lohman, P. Karamchandani, and C. Scott (2004), Global source attribution for mercury deposition in the United States, *Environ. Sci. Technol.*, *38*, 555–569.
Selin, N. E., D. J. Jacob, R. J. Park, R. M. Yantosca, S. Strode, L. Jaeglé, and D. Jaffe (2007), Chemical cycling and deposition of atmospheric mercury: Global constraints from observations, *J. Geophys. Res.*, *112*, D02308, doi:10.1029/2006JD007450.
Shia, R.-L., C. Seigneur, P. Pai, M. Ko, and N. D. Sze (1999), Global simulation of atmospheric mercury concentrations and deposition fluxes, *J. Geophys. Res.*, *104*, 23,747–23,760.
Slemr, F. (1996), Trends in atmospheric mercury concentrations over the Atlantic Ocean and at the Wank Summit, and the resulting constraints on the budget of atmospheric mercury, in *Global and Regional Mercury Cycles: Sources, Fluxes, and Mass Balances*, edited by W. Baeyens, R. Ebinghaus, and O. Vasiliev, pp. 33–84, Springer, New York.
Slemr, F., and E. Langer (1992), Increase in global atmospheric concentrations of mercury inferred from measurements over the Atlantic Ocean, *Nature*, *355*, 434–437.

Slemr, F., W. Junkermann, R. W. H. Schmidt, and R. Sladkovic (1995), Indication of change in global and regional trends of atmospheric mercury concentrations, *Geophys, Res. Lett.*, *22*, 2143–2146.

Slemr, F., E.-G. Brunke, R. Ebinghaus, C. Temme, J. Munthe, I. Wängberg, W. Schroeder, A. Steffen, and T. Berg (2003), Worldwide trend of atmospheric mercury since 1997, *Geophys. Res. Lett.*, *30*(10), 1516, doi:10.1029/2003GL016954.

Sommar, J., K. Gårdfeldt, D. Strömberg, and X. Feng (2001), A kinetic study of the gas-phase reaction between the hydroxyl radical and atomic mercury, *Atmos. Environ.*, *35*, 3049–3054.

Temme, C., F. Slemr, R. Ebinghaus, and J. W. Einax (2003), Distribution of mercury over the Atlantic Ocean in 1996 and 1999–2001, *Atmos. Environ.*, *37*, 1889–1897.

Wängberg, I., S. Schmolke, P. Schager, J. Munthe, R. Ebinghaus, and Å. Iverfeldt (2001), Estimates of air-sea exchange of mercury in the Baltic Sea, *Atmos. Environ.*, *35*, 5477–5485.

Wolfe, M. F., S. Schwarzbach, and R. A. Sulaiman (1998), Effects of mercury on wildlife: A comprehensive review, *Environ. Toxicol. Chem.*, *17*, 146–160.

D. J. Jacob, R. J. Park, N. E. Selin, and R. M. Yantosca, Division of Engineering and Applied Sciences, Harvard University, Cambridge, MA 02138, USA.

L. Jaeglé and S. A. Strode, Department of Atmospheric Sciences, University of Washington, Box 351640, Seattle, WA 98195-1640, USA. (jaegle@atmos.washington.edu; sstrode@atmos.washington.edu)

R. P. Mason, Department of Marine Sciences, University of Connecticut, Groton, CT 06340, USA.

F. Slemr, Air Chemistry Division, Max-Planck-Institute for Chemistry, Joh.-Joachim-Becher-Weg 27, D-55128, Mainz, Germany.